Towards Personalised Therapy in Atrial Fibrillation: The Role of Patient-Specific Fibrosis

Semhar B Misghina[1], Alexander M Zolotarev[1], Elisa Rauseo[1], Carlos E Barrera[1], Steven A Niederer[2], Gregory Slabaugh[1], Gernot Plank[3], Nay Aung[1], Steffen E Petersen[1], Patricia B Munroe[1], Edward J Vigmond[4], Caroline H Roney[1]

[1] Queen Mary University of London, London, United Kingdom
[2] Imperial College London, London, United Kingdom
[3] Medical University of Graz, Graz, Austria
[4] University of Bordeaux, Bordeaux, France

Abstract

Current Atrial Fibrillation (AF) treatments often follow a one-size-fits-all approach, overlooking the effect of inter-patient variability in fibrosis on therapeutic outcomes. A computational framework integrating patient-specific anatomical and fibrotic data, with electrophysiology, is needed to personalise therapy selection at a scale.

Patient-specific biatrial models (n=69) were created from late gadolinium-enhanced MRI (LGE-MRI) images by manual segmentation. Pre-processing included fibrosis quantification and integration of atrial fibre data from a fibre atlas. PVI was simulated as non-conductive lesions around the pulmonary veins, and three anti-arrhythmic drugs (vernakalant, amiodarone [acute, chronic], and flecainide) were virtually administered. Finite element simulations were performed and post-processed to compare therapy-induced AF termination with and without fibrosis.

The success rates of anti-arrhythmic drugs in fibrotic anatomies closely matched with the ESC 2024 guideline acute success rates: flecainide had the highest rate (67%, ESC 50%-60%), followed by vernakalant (58%, ESC 50%) and amiodarone (35% [acute], 45% [chronic]; ESC 44%).

This study demonstrates the benefit of fibrosis-driven personalisation in guiding therapeutic decisions.

1. Introduction

Atrial Fibrillation (AF) is a prevalent cardiac arrhythmia characterised by disorganised atrial electrical activity [1]. Clinical management includes anti-arrhythmic drugs (AADs) and catheter ablation, but both have variable efficacy and high recurrence rates. Catheter ablation, including pulmonary vein isolation (PVI), remains the first-line interventional treatment; however, up to one-third of patients relapse within a year [1]. These limitations highlight the need for more personalised therapies that account for inter-patient heterogeneity in fibrosis and anatomy. Fibrosis plays a key role in AF progression, disrupting conduction pathways and facilitating re-entrant circuits that sustain AF [1]. Prior studies have shown that fibrotic heterogeneity influences therapy outcomes, yet current approaches often rely on generalised patient cohorts or primarily evaluate a limited range of AADs [2]. Our approach increases personalisation by constructing biatrial models and fibrotic masks at a scale from LGE-MRI data. Advances in LGE-MRI imaging have enabled fibrosis quantification; however, the effect of patient-specific fibrosis on treatment response to AADs and PVI remains unclear. This study aims to evaluate the effect of patient-specific fibrosis on the success rates of AADs and PVI using personalised biatrial models derived from imaging data.

We constructed 69 patient-specific anatomical models from LGE-MRI images by manual segmentation and integrated atrial fibre data from a fibre atlas. Patient-specific fibrosis maps were generated from LGE-MRI images to quantify fibrotic burden. PVI was simulated, and three AADs were virtually administered. Finite element simulations were performed and post-processed to assess the AF termination rates of AADs, PVI, and their combination in fibrotic and non-fibrotic cases.

2. Methods

2.1. Patient-Specific Model Generation

The patient cohort included 69 AF individuals from the STACOM 2018 Left Atrial Segmentation Challenge dataset (https://www.cardiacatlas.org/atriaseg2018-challenge/). The dataset includes 3D LGE-MRI images with anisotropic resolutions of $0.625 \times 0.625 \times 1.25$ mm^3 and dimensions of $576 \times 576 \times 88$ or $640 \times 640 \times 88$ pixels

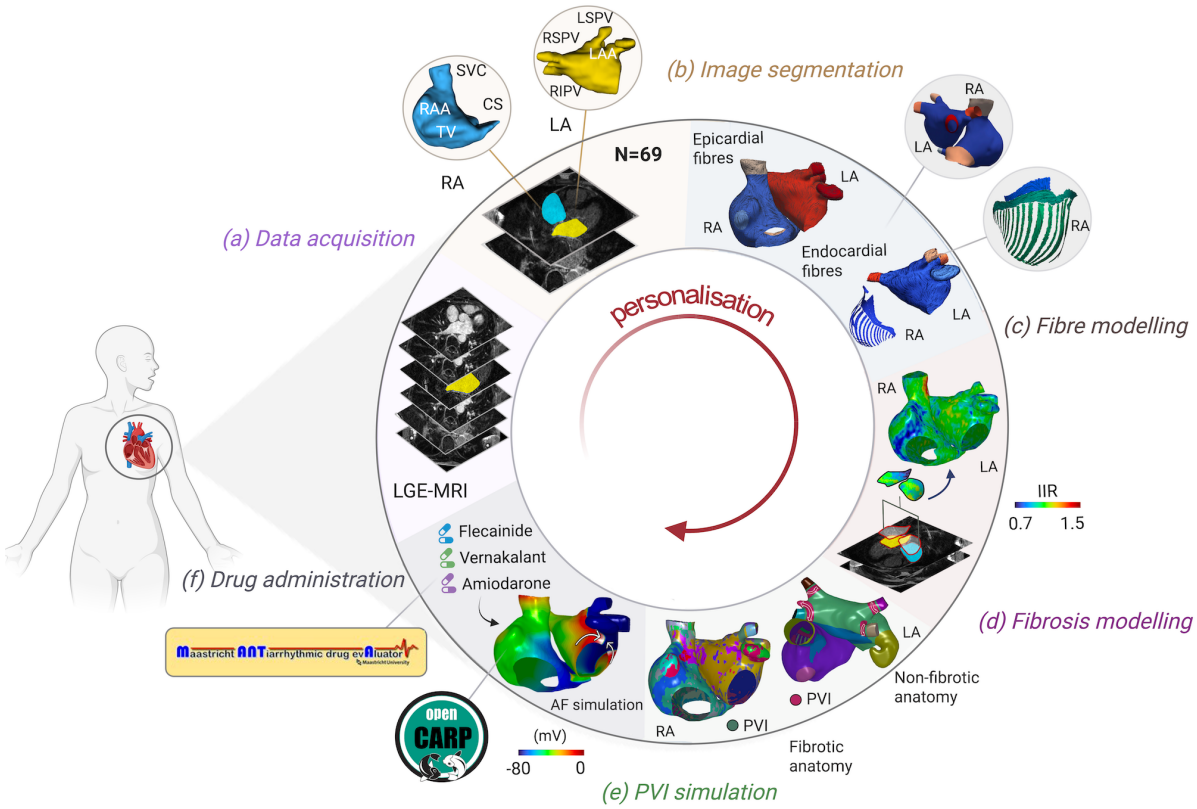

Figure 1. Biatrial model generation and AF therapeutic simulation workflow: (a) LGE-MRI data acquisition (69 patients), (b) manual segmentation of right atrium (RA) and left atrium (LA) to create biatrial anatomies, (c) integration of atrial fibre data from the Labarthe et al. [3] atlas, (d) LGE intensity registration to generate fibrotic masks, (e) PVI simulated as non-conductive rings in fibrotic and non-fibrotic anatomies, (f) drug administration using ionic current block (%) from MANTA in OpenCarp. Finite element simulations were performed to compare AF termination rates across therapies.

(88 slices) (Fig.1(a)) [4]. Manually segmented left atrial (LA) blood-pool masks were provided for each patient. All participants provided informed consent, and the study was approved by the University of Utah and University Hospital of Dijon institutional review boards [4].

Biatrial anatomical models were created by manually segmenting LGE-MRI images using 3D Slicer software (Fig.1(b)). The right atrium (RA) blood pool was annotated in each 2D slice, and the resulting 3D RA models were exported for pre-processing. The 3D RA segmentations were validated against pre-labelled LGE-MRI atlases, reviewed by clinicians, and combined with 3D LA models to construct patient-specific biatrial anatomies.

2.1.1. Pre-Processing & Fibrosis Modelling

Pre-processing was performed to generate meshes suitable for electrophysiological modelling. First, closed surface meshes were clipped at the pulmonary veins (PV), mitral valve, coronary sinus (CS), tricuspid valve, and vena cava (VC). Following Roney et al. [5], anatomical landmarks were selected to identify atrial regions and calculate atrial coordinates for fibre modelling [5]. Laplace-Dirichlet solutions were computed in OpenCARP to automatically delineate the PV, VC, LA appendage, RA appendage, and CS on the biatrial meshes.

Personalised bilayer shells were then constructed by integrating atrial structures and fibre data from the Labarthe et al. [3] atlas using universal atrial coordinates and *atrialmtk* (https://github.com/pcmlab/atrialmtk) (Fig.1(c)) [5]. This incorporated endocardial and epicardial fibres, pectinate muscles, crista terminalis, Bachmann's bundle, the sinoatrial node, and interatrial pathways.

Fibrotic distributions were mapped by projecting LGE-MRI image intensity ratios onto the meshes (Fig.1(d)). The atrial wall intensities were normalised by dividing each value by the mean blood pool intensity [6]. The wall intensities were computed by overlaying the atrial surface with the LGE-MRI and calculating the maximum projection along the normal direction of each mesh element [6] [7]. For electrophysiological modelling, conductivity values for mild, moderate, and severe fibrosis were assigned.

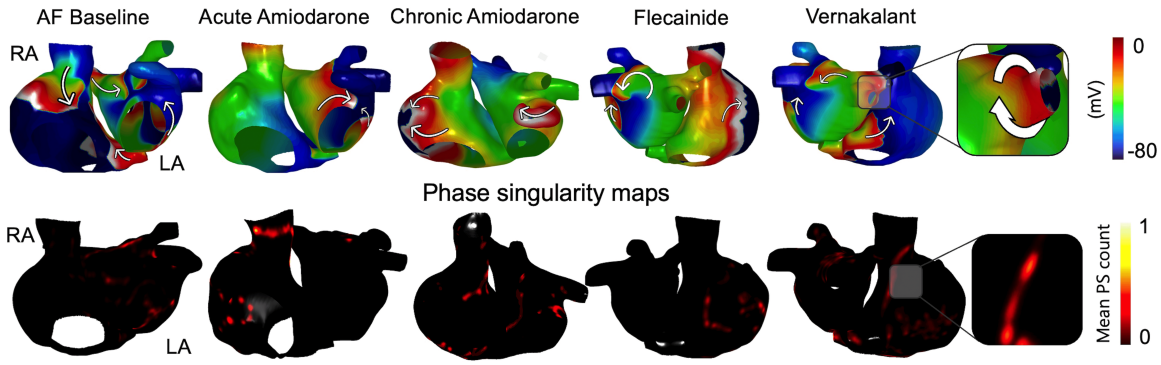

Figure 2. Finite element simulations and PS maps showing the effect of AADs on AF dynamics in fibrotic anatomies. The arrows indicate wavefront propagation patterns and the colour bars show transmembrane potential and mean PS count.

2.2. Therapeutic Simulation Protocols

Following Roney et al. [8], PVI was simulated by creating circumferential non-conductive lesions at a 6mm distance threshold from the left and right LA-PV antra (tissue conductivity set to 0.001 S/m) (Fig.1(e)). To simulate drug effects, we virtually administered vernakalant, amiodarone (acute and chronic), and flecainide at therapeutic concentrations (Table 1) (Fig.1(f)) [9]. The Maastricht Antiarrhythmic Drug Evaluator (MANTA) was used to calculate ionic current block percentages based on these concentrations, using the Courtemanche et al. [10] ionic cell model (Table 1) [11]. It adjusts maximal conductance for each AADs using a sigmoidal Hill curve with previously reported IC_{50} values.

Table 1. Ionic current blocks (%). Key ion channels: I_{Kr} (rapid K^+); I_{to} (transient K^+); I_{NCX} (Na^+/Ca^{2+} exchanger); I_{Na} (Na^+); I_{CaL} (L-type Ca^{2+}); I_{Ks} (slow K^+); I_{Kur} (ultra-rapid K^+).

Drugs	Dose	I_{Kr}	I_{to}	I_{NCX}	I_{Na}	I_{CaL}	I_{Kur}	I_{Ks}
Acute amiodarone	3.0 μM	50	47	46	37	60	0	2
Chronic amiodarone	3.0 μM	68	47	46	37	60	0	24
Flecainide	2.0 μM	65	27	0	31	9	50	0
Vernakalant	10 μM	33	40	0	10	10	40	0

Finite element simulations were performed to compare the effect of therapies on AF dynamics in fibrotic and non-fibrotic cases (Fig.1(f)). The Courtemanche et al. [10] cell model and the OpenCARP monodomain solver were used for 15s of excitation propagation [7]. The ionic properties were modified to mimic AF-induced electrical remodelling (I_{Kur}, I_{to}, I_{CaL} reduced by 50%, 50%, and 70%, respectively). AF was initiated through seeding four spiral wave re-entries [7]. Patients with sustained AF (>10s) were administered AADs, with ionic current block (%) from MANTA applied in OpenCARP to simulate drug effects. Simulations were performed for AADs alone, PVI alone, and their combination, for both fibrotic and non-fibrotic cases (Fig.2). Drug efficacy was measured as the percentage of patients achieving AF termination (sinus rhythm). Phase singularity (PS) maps were generated to identify re-entry sites and AF wavefront break-up under different treatments.

3. Results

The success rates of AADs in fibrotic anatomies closely matched with the European Society of Cardiology (ESC) 2024 guideline acute success rates (Table 2): flecainide had the highest rate, followed by vernakalant and amiodarone. However, combining PVI with AADs did not significantly improve success rates over AADs alone in either anatomical state. PVI alone had low success rates (5% [non-fibrotic], 2% [fibrotic]); however, these rates reflect only substrate modification and exclude ectopic trigger elimination, which may contribute to better long-term outcomes.

Table 2. Comparison of success rates between ESC 2024 and in-silico simulations for non-fibrotic vs fibrotic.

Drugs	**Acute success rates (%)**		
	In-silico		
	Non-Fibrotic	**Fibrotic**	**ESC 2024**
Acute amiodarone	14	35	44
Chronic amiodarone	14	45	44
Flecainide	44	67	50–60
Vernakalant	30	58	50

A negative correlation between RA surface area (SA) and AAD success rates (ρ=-0.42, $p<0.05$) was found, suggesting that larger RA SA reduces AAD effectiveness. Fibrotic cases had significantly higher baseline PS counts than non-fibrotic cases ($p<0.001$), indicating that fibrosis may create a more unstable AF substrate. In fibrotic cases, PS clusters initially spread across the LA but later concen-

trated in the RA septum and LA roof after AAD administration. PS localisation increased in the RA with all AAD treatments, suggesting RA SA may be a biomarker in predicting treatment outcomes. Flecainide treatment resulted in exclusive PS localisation in the RA, which may explain its superior efficacy in both fibrotic and non-fibrotic cases.

4. Discussion

This study demonstrates that integrating patient-specific anatomical and fibrotic data, with electrophysiological data can improve therapeutic outcomes. Incorporating personalised fibrotic data resulted in AAD success rates closely matching with ESC 2024 guidelines and previous clinical trials. For vernakalant, simulated efficacy (58%) was consistent with Pohjantähti-Maaroos et al. [12] at 59%; for flecainide, simulated efficacy (67%) matched clinical trials (59% by Botto et al. [13]; 75% by Boriani et al. [14]. Compared to Dasí et al. [9], we observed similar efficacies in fibrotic cases with the same dosage: vernakalant (42%), flecainide (38%-78%), and amiodarone (11%-89%). Dasí et al. [9] used 800 virtual atria and modelled fibrosis as low-voltage isotropic areas, virtually administering four AADs. These differences may reflect increasing degrees of personalisation, with biatrial meshes constructed from imaging data and fibrotic masks from LGE-MRI. Our results showed low efficacy with PVI alone (5% [non-fibrotic], 2% [fibrotic]) and a non-significant effect of combination therapy (AADs + PVI), likely due to substrate modification alone and exclusion of ectopic trigger elimination. These results align with Roney et al. [8], who found that termination rates in persistent AF depend on factors such as ectopic beats and electrical driver locations. Similarly, the DECAAF II trial found no significant improvement in AF recurrence rates when adding fibrosis-guided ablation to PVI in patients with persistent AF [1].

Our work is limited by modelling fibrosis solely as spatial conductivity variations, which may not fully capture its structural and functional complexity. We also have not compared with other fibrosis modelling methods, which could influence the generalisability and predictive power of the framework. The low success rates of PVI alone reflect substrate modification only without considering ectopic trigger elimination. Future studies will model fibrosis using probabilistic percolation to assess its effect on therapeutic outcomes. We also plan to assess AF reinducibility with pacing protocols to compare acute and long-term outcomes and predict drug-modulated AF recurrence.

5. Conclusion

Our study demonstrates the benefit of fibrosis-driven personalisation in guiding AF therapy selection.

Acknowledgments

This research was funded by a UKRI Future Leaders Fellowship (MR/W004720/1).

References

[1] Marrouche N, et al. Effect of mri-guided fibrosis ablation vs conventional catheter ablation on atrial arrhythmia recurrence in persistent atrial fibrillation. JAMA 2022; 327(23):2296–2305.

[2] Hwang T, et al. Clinical usefulness of digital twin guided virtual amiodarone test in patients with atrial fibrillation ablation. NPJ Digit Med 2024;7(1):297.

[3] Labarthe S, et al. A bilayer model of human atria: mathematical background, construction, and assessment. Europace 2014;16(suppl_4):iv21–iv29.

[4] McGann C, et al. Atrial fibrillation ablation outcome is predicted by left atrial remodeling on mri. Circ Arrhythm Electrophysiol 2014;7(1):23–30.

[5] Roney CH, et al. Constructing bilayer and volumetric atrial models at scale. Interface Focus 2023;13(6):20230038.

[6] Solís-Lemus JA, et al. Evaluation of an open-source pipeline to create patient-specific left atrial models. Comput Biol Med 2023;162:107009.

[7] Roney CH, et al. Predicting atrial fibrillation recurrence by combining population data and virtual cohorts. Circ Arrhythm Electrophysiol 2022;15(2):e010253.

[8] Roney CH, et al. Variability in pulmonary vein electrophysiology and fibrosis determines arrhythmia susceptibility. PLoS Comput Biol 2018;14(5):e1006166.

[9] Dasí A, et al. What determines the optimal pharmacological treatment of atrial fibrillation? J Physiol 2023; 601(18):4013–4032.

[10] Courtemanche M, et al. Ionic mechanisms underlying human atrial action potential properties: insights from a mathematical model. Am J Physiol Heart Circ Physiol 1998; 275(1):H301–H321.

[11] Sutanto H, et al. Manta: A computational tool for better understanding antiarrhythmic drugs. Pharmacol Res 2019; 148:104444.

[12] Pohjantähti-Maaroos H, et al. Intravenous vernakalant in comparison with intravenous flecainide in the cardioversion of recent-onset atrial fibrillation. Eur Heart J Acute Cardiovasc Care 2019;8(2):114–120.

[13] Botto GL, et al. Regular ventricular rhythms before conversion of recent onset atrial fibrillation to sinus rhythm. Pacing Clin Electrophysiol 1994;17(11):2114–2117.

[14] Boriani G, et al. Conversion of recent-onset atrial fibrillation to sinus rhythm: effects of different drug protocols. Pacing Clin Electrophysiol 1998;21(11):2470–2474.

Address for correspondence:

Semhar Misghina
Queen Mary University of London, UK
s.b.misghina@qmul.ac.uk